

# QCD thermodynamics with $O(a)$ improved Wilson fermions at $N_f = 2$

---

**Bastian B. Brandt\***

*Institut für theoretische Physik,  
Universität Regensburg, D-93040 Regensburg  
E-mail: [bastian.brandt@physik.uni-regensburg.de](mailto:bastian.brandt@physik.uni-regensburg.de)*

**Anthony Francis, Harvey B. Meyer and Hartmut Wittig**

*PRISMA Cluster of Excellence, Institut für Kernphysik  
and Helmholtz Institut Mainz,  
Johannes Gutenberg-Universität Mainz, D-55099 Mainz*

**Owe Philipsen**

*Institut für Theoretische Physik,  
Goethe-Universität, D-60438 Frankfurt am Main*

We present an update of our study of the phase diagram of two-flavour QCD at zero baryon density with dynamical  $O(a)$  improved Wilson quarks. All simulations are done on lattices with a temporal extent of  $N_t = 16$  and spatial extent  $L = 32, 48$  and  $64$ , ensuring that discretisation effects are small and finite size effects can be controlled. In the approach to the chiral limit we currently have three scans with pion masses between  $540$  and  $200$  MeV. In this proceedings article the focus is on the new scan at  $m_\pi = 200$  MeV and the measurement of screening masses. We also present first results concerning a test of scaling in the approach to the chiral limit and the chiral extrapolation of the difference of screening masses in scalar and pseudoscalar channels, which provides a measure for the strength of the anomalous breaking of the  $U_A(1)$  symmetry.

*31st International Symposium on Lattice Field Theory LATTICE 2013  
July 29 – August 3, 2013  
Mainz, Germany*

---

\*Speaker.

## 1. Introduction

Due to the continued progress in the field of lattice QCD at finite temperature in the last few years, most of the features of the phase diagram in the  $\{m_{ud}, m_s, T\}$  parameter space at vanishing chemical potential are by now rather well understood (for a review see [1]). One of the most prominent remaining issues at vanishing chemical potential concerns the behaviour of the chiral critical line with increasing strange quark mass. There are two possible scenarios [2, 3]: Either the chiral critical line reaches the  $m_{ud} = 0$  axis at some tri-critical point, so that from this point on the transition is of second-order in the chiral limit, or the chiral critical line continues at non-vanishing  $m_{ud}$  up to infinitely heavy strange quarks, leaving a first-order transition at  $m_{ud} = 0$ . The universality class of the chiral transition in the second-order scenario depends on the strength of the anomalous breaking of the  $U_A(1)$  symmetry [2, 3, 4]. In case of a strong breaking the transition is in the 3d  $O(4)$  universality class [4, 5], for a weak breaking in the 3d  $U(2) \times U(2) \rightarrow U(2)$  universality class [3, 4]. The first-order scenario is expected to be realised for a nearly restored  $U_A(1)$  symmetry.

Here we present an update of our study [6, 7, 8] concerning the order of the transition in the chiral limit of the two-flavour theory with non-perturbatively  $O(a)$  improved Wilson fermions. To investigate the approach to the chiral limit with control over the main systematic effects we use  $N_t = 16$  throughout, thereby reducing the cutoff effects to a minimum, and aim at simulations at several pion masses below 300 MeV at three different volumes each. In this proceedings article the focus will be on the measurements of screening masses and first attempts to extrapolate our results to the chiral limit. For details concerning strategy and setup we refer to our earlier publications. Another aspect of our project is the measurement of plasma properties in the transition region and above [9, 10, 11], which will not be covered here.

## 2. Temperature scans and transition temperatures

### 2.1 Scan setup

Our simulations use non-perturbatively  $O(a)$  improved Wilson fermions [12] with two degenerate dynamical quarks and the Wilson plaquette action. The configurations are generated with deflation accelerated DD-HMC [13, 14] and MP-HMC [15] algorithms. The lattice sizes are chosen to be  $16 \times 32^3$ ,  $48^3$  and  $64^3$  to suppress cutoff effects and to enable the extrapolation to the thermodynamic limit. To scan in temperature we vary the bare coupling  $\beta$  either at fixed hopping parameter  $\kappa$  (for  $m_\pi > 300$  MeV) or fixed renormalised quark mass (for  $m_\pi < 300$  MeV). Scale setting, renormalisation and tuning for lines of constant physics is done using input from CLS [16, 17, 18]. To determine the mass scale we use the renormalised PCAC mass in the  $\overline{\text{MS}}$  scheme at  $\mu = 2$  GeV measured directly on our finite-T ensembles (see [11]).

Our main observables concerning the transition are the real part of the APE-smear Polyakov loop ( $L_{SM}$ ), the subtracted chiral condensate [19, 20] ( $\langle \bar{\psi}\psi \rangle_{\text{sub}}$ ) as defined in [10] and the associated susceptibilities. At the moment those observables are unrenormalised. The error analysis has been done using the bootstrap method with 1000 bins.

scan	Lattice	$\kappa/m_{ud}$ [MeV]	$T$ [MeV]	$\tau_{Up}$ [MDU]	MDUs	$T_C$ [MeV]	$(m_{ud})_C$ [MeV]
<b>B1<math>_{\kappa}</math></b>	$16 \times 32^3$	0.136500	190 – 275	$\sim 10$	$\sim 20000$	245 (7)(6)	45 (2)(2)
<b>B3<math>_{\kappa}</math></b>	$16 \times 64^3$	0.136500	240 – 250	$\sim 46$	$\sim 16000$		
<b>C1</b>	$16 \times 32^3$	$\sim 14.5$	150 – 250	$\sim 8$	$\sim 12000$	211 (5)(3)	14.3 (14)(9)
<b>D1</b>	$16 \times 32^3$	$\sim 7.5$	175 – 250	$\sim 8$	$\sim 10000$	193 (7)(5)	7.6 (19)(7)

**Table 1:** Scans at  $N_t = 16$  at constant  $\kappa$  (subscript  $\kappa$ ) and constant renormalised quark mass. Listed is the temperature range in MeV, the integrated autocorrelation time of the plaquette  $\tau_{Up}$ , the number of molecular dynamics units (MDUs) used for the analysis (the measurement frequency being 4 MDUs) and the parameters, temperature  $T_C$  and quark mass  $(m_{ud})_C$ , at the critical point. For the latter, the first uncertainty is obtained from the spread of results in the transition region. The second error contains the uncertainties of the individual measurements, scale setting and renormalisation.

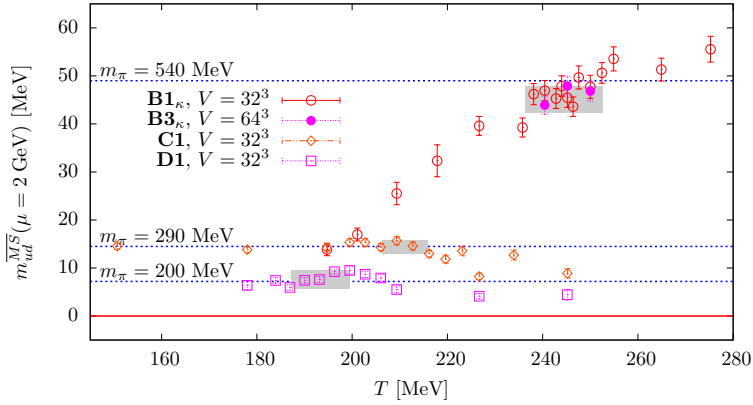


**Figure 1:** Simulation points in the  $\{m_{ud}, T\}$  parameter space. The grey areas mark the crossover regions.

## 2.2 Transition temperatures

So far our set of temperature scans at  $N_t = 16$  consists of three scans with the simulation parameters given in table 1 and the associated simulation points in the  $\{m_{ud}, T\}$  parameter space are displayed in figure 1. Scans **B1 $_{\kappa}$** , **B3 $_{\kappa}$**  and **C1** have already been presented in our earlier publications [6, 7, 8] and the resulting transition temperatures are given in table 1, too <sup>1</sup>. The scan **D1** is new and we show the results for the Polyakov loop and the susceptibility of the subtracted chiral condensate in figure 2 in comparison to the results from scan **C1**.

The qualitative behaviour of the Polyakov loop is similar in both scans with a slight shift towards smaller temperature values for scan **D1**, indicating a smaller transition temperature, in agreement with the expectations for smaller quark masses. The susceptibilities of the subtracted condensate in the two scans show a decrease when going to higher temperatures with a peak on top, due to the superposition of the general  $T = 0$  behaviour (which is not subtracted here) and the thermal effects. The transition temperature is extracted from the peak using a fit to a Gaussian (see [8]). For scan **D1** the susceptibility still shows rather large fluctuations in the estimated transition region and we currently increase statistics in this region to obtain a better signal for  $\chi_{\langle\bar{\psi}\psi\rangle_{\text{sub}}}$ . Nevertheless, all observables unambiguously indicate critical behaviour in the region between 186

<sup>1</sup>The results for scan **C1** in table 1 and figure 2 have been obtained with enlarged temperature range and statistics in comparison to our earlier results presented in [8] and differ slightly.

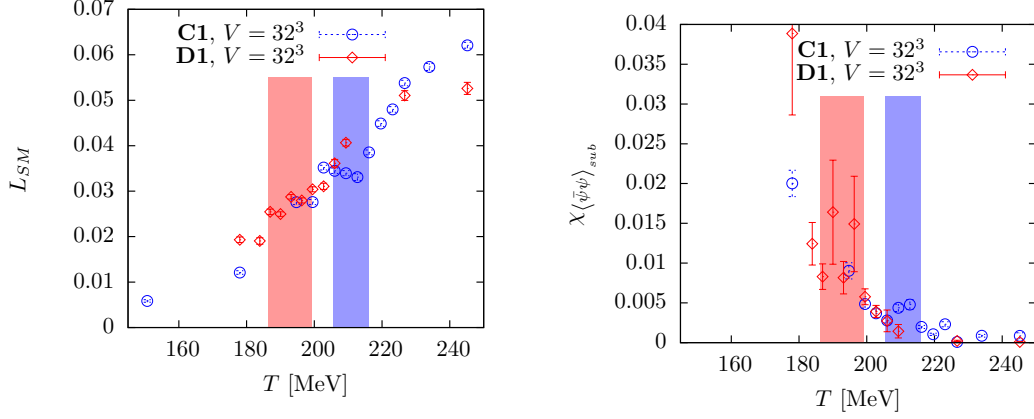


**Figure 2:** Results for the smeared Polyakov Loop (left) and the susceptibility of the subtracted chiral condensate (right) from scans **C1** and **D1**. The filled areas mark the estimates for the transition regions.

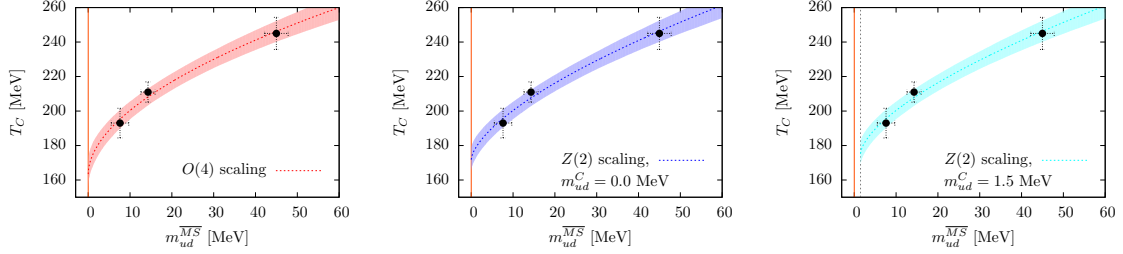


**Figure 3:** Results for the scaling of the transition temperature using the critical exponents of the  $O(4)$  (left) and the  $Z(2)$  universality class (middle and right) at different values of  $m_{ud}^C$ .

and 200 MeV, which we identify as the transition region in table 1.

### 2.3 Scaling of the critical temperature

With three transition temperatures at our disposal we can perform a first scaling analysis in the approach to the chiral limit. In the continuum scaling (which is the one realised for Wilson fermions due to explicit chiral symmetry breaking at finite lattice spacing) the transition temperature changes with the renormalised quark mass according to [21, 22]

$$T_C(m_{ud}) = T_C(0) \left[ 1 + C m_{ud}^{1/(\delta\beta)} \right], \quad (2.1)$$

Here  $\delta$  and  $\beta$  are the critical exponents associated with the universality class of the critical point. This scaling will be realised up to scaling violations in the approach to a critical point at  $m_{ud} = 0$ , i.e. in either of the second-order scenarios depicted in the introduction. The situation is more complicated in the case of a first-order transition in the chiral limit, due to the absence of an order parameter at the  $Z(2)$  critical point at finite  $m_{ud} = m_{ud}^C$  (for a recent discussion see [23]). Assuming that eq. (2.1) also holds in the approach to this critical point, one can simply replace  $m_{ud} \rightarrow m_{ud} - m_{ud}^C$  in the associated scaling analysis.

The precision of our data does not allow to constrain either the critical exponents and/or  $m_{ud}^C$ , so that we are left with comparing the agreement with the data using either of the critical exponents and different cases for  $m_{ud}^C$  (here  $m_{ud}^C=0$  and 1.5 MeV) in the first-order scenario. The results of

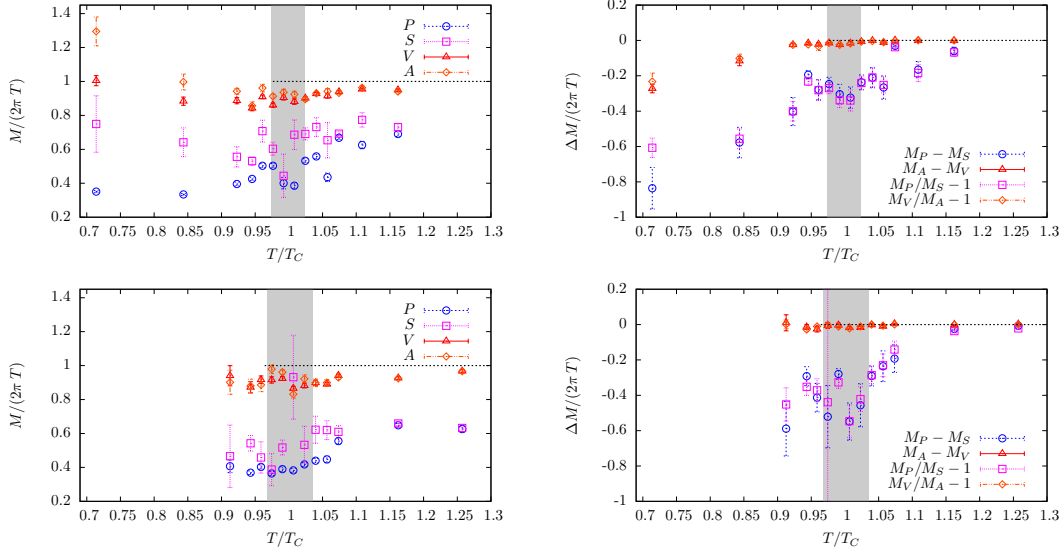


**Figure 4:** **Left:** Temperature dependence of screening masses in  $P$ ,  $S$ ,  $V$  and  $A$  channels for scans **C1** (top) and **D1** (bottom). The dashed line indicates the asymptotic value of  $M = 2\pi T$  for  $T \rightarrow \infty$ . **Right:** Screening mass differences in  $S$  and  $P$  and  $A$  and  $V$  channels in units of  $2\pi T$ . The two sets of points have been extracted from fits to the  $x^3$ -dependence of the mass difference and the mass ratio, respectively.

the fits with fit parameters  $T_C(0)$  and  $C$  are shown in figure 3. Since the critical exponents of the  $O(4)$  and the  $U(2) \times U(2) \rightarrow U(2)$  scenario [4] are too similar to be distinguished, we have only shown the analysis for the  $O(4)$  case. The plots demonstrate that all scenarios are compatible with the data. This is not surprising given the still relatively large quark masses used for the analysis. Similar problems to distinguish the scenarios from scaling alone have been reported by the tmfT collaboration with pion masses between 300 and 500 MeV [23].

### 3. Screening masses and $U_A(1)$ symmetry breaking

To investigate the chiral symmetry restoration pattern we look at the degeneracy of iso-vector screening masses in pseudoscalar ( $P$ ), scalar ( $S$ ), vector ( $V$ ) and axial vector ( $A$ ) channels, the former two being directly related to the breaking of the  $U_A(1)$  symmetry [24]. The associated correlation functions have been measured each 40 and 20 MDUs, for scans **C1** and **D1**, respectively, using 15 point sources at different positions for each configuration.

The temperature dependence of the screening masses is shown in figure 4 (left) in comparison with the respective mass splittings (right)<sup>2</sup>. The screening masses start from the expected splittings from the meson spectrum at zero-temperature (at least for scan **C1** where results at lower temperatures are available). In the approach to  $T_C$  the screening masses in  $S$  and  $A$  channels become smaller while the ones in  $P$  and  $V$  channels initially remain constant before  $M_P$  grows rapidly. This is in agreement with the results obtained with staggered fermions [25, 26]. Around  $T_C$  the masses in  $V$  and  $A$  channels become degenerate, in agreement with the restoration of the chiral  $SU_A(2)$

<sup>2</sup>The splittings are obtained from a fit to either the effective mass for the difference  $\Delta M$  or a fit to the ratio of effective masses directly. This provides a more solid estimate for the mass splittings since the plateau for these quantities are reached earlier and parts of the fluctuations cancel.

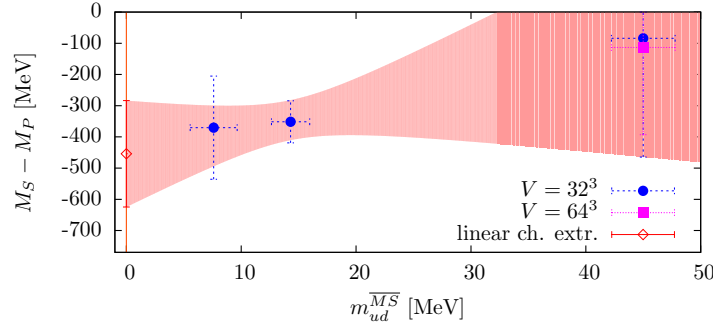


**Figure 5:** Chiral extrapolation of  $M_S - M_P$  in MeV on the  $32^3$  volume in the thermal transition region using a linear function in  $m_{ud}$ . Also shown is the result of scan **B3 $\kappa$**  at a volume of  $64^3$ .

symmetry, and are about 10 % smaller than the asymptotic value. In contrast, the masses of  $P$  and  $S$  channels remain disparate, signaling the persistent breaking of the  $U_A(1)$  symmetry, and are in the region of 40 to 60 % of the  $2\pi T$  limit. Above  $T_C$  all screening masses approach the asymptotic limit from below, which might be a remnant of the relatively small volume with  $N_s/N_t = 2$  (see [27]). Finite size effects will be studied once the larger volumes become available. The masses in  $P$  and  $S$  channels become degenerate at about  $1.25 T_C$  for scan **D1** (for scan **C1** they are still non-degenerate at  $T/T_C \approx 1.17$ ) which coincides with the result at  $m_\pi = 200$  MeV from  $N_f = 2 + 1$  domain wall [28, 29] and staggered fermion simulations [25, 26].

Relevant for the order of the transition is the strength of the breaking of  $U_A(1)$  in the chiral limit which can be assessed by performing a chiral extrapolation for some suitable measure. Here we use the average of the mass difference in  $S$  and  $P$  channels in the transition region as a measure for the strength of the breaking, which we then extrapolate to the chiral limit. The results for scans **B1 $\kappa$** , **C1** and **D1** are shown in figure 5 together with a linear extrapolation in  $m_{ud}$ . As can be seen from the plot, our current results strongly suggest a non-vanishing difference at  $m_{ud} = 0$ . However, to address the question of the order of the transition one still has to clarify the criterion which determines a ‘strong’ breaking. It appears that a proper criterion should make contact with the strength of the breaking at  $T = 0$ , so that the breaking at  $T_C$  can be expressed in relation to this. A possible measure is provided by the mass of the iso-vector scalar particle at  $T = 0$  in the chiral limit. A comparison with this quantity will be done in future publications.

#### 4. Conclusions and perspectives

In this proceedings article we have presented the current status of our project to investigate the order of the transition in the chiral limit at  $N_f = 2$ . The available results for the transition temperatures at three different pion masses between 200 and 500 MeV at  $N_t = 16$  allow for a first test of critical scaling in the approach to the chiral limit. As expected, using the scaling alone, with the current set of still relatively large pion masses, is not sufficient to distinguish between the two scenarios. Scans at smaller pion masses are in preparation and will hopefully improve the situation. As another source of information we have extracted the difference of screening masses in  $S$  and  $P$  channels which is a measure for the strength of the breaking of the  $U_A(1)$  symmetry. The first naive chiral extrapolation of this quantity shows that the effect has the tendency to become stronger in

the approach to the chiral limit. However, simulations at smaller pion masses and at larger volumes are needed to confirm this statement.

**Acknowledgements:** The simulations were done on the WILSON and LC2 clusters at the University of Mainz, the FUCHS cluster at the University of Frankfurt and on JUROPA and JUGENE at FZ Jülich under project number HMZ21.

## References

- [1] M. P. Lombardo, PoS LATTICE **2012** (2012) 016 [arXiv:1301.7324]
- [2] R. D. Pisarski and F. Wilczek, Phys. Rev. D **29** (1984) 338
- [3] A. Butti, A. Pelissetto and E. Vicari, JHEP **0308** (2003) 029 [hep-ph/0307036]
- [4] A. Pelissetto and E. Vicari, arXiv:1309.5446
- [5] K. Rajagopal and F. Wilczek, Nucl. Phys. B **399** (1993) 395 [hep-ph/9210253]
- [6] B. B. Brandt, *et al.*, PoS LATTICE **2010** (2010) 172 [arXiv:1008.2143]
- [7] B. B. Brandt, *et al.*, AIP Conf. Proc. **1343** (2011) 516 [arXiv:1011.6172]
- [8] B. B. Brandt, *et al.*, PoS LATTICE **2012** (2012) 073 [arXiv:1210.6972]
- [9] B. B. Brandt, *et al.*, JHEP **1303** (2013) 100 [arXiv:1212.4200]
- [10] B. B. Brandt, *et al.*, PoS ConfinementX (2012) 186 [arXiv:1302.0675]
- [11] B. B. Brandt, A. Francis and H. B. Meyer, arXiv:1310.5160
- [12] B. Sheikholeslami and R. Wohlert, Nucl. Phys. B **259** (1985) 572
- [13] M. Lüscher, Comput. Phys. Commun. **165** (2005) 199 [hep-lat/0409106]
- [14] M. Lüscher, JHEP **0712** (2007) 011 [arXiv:0710.5417]
- [15] M. Marinkovic and S. Schaefer, PoS LATTICE **2010** (2010) 031 [arXiv:1011.0911]
- [16] B. Leder, *et al.* [ALPHA Collaboration], PoS LATTICE **2010** (2010) 233 [arXiv:1012.1141]
- [17] P. Fritzsch, *et al.*, Nucl. Phys. B **865** (2012) 397 [arXiv:1205.5380]
- [18] B. B. Brandt, A. Jüttner and H. Wittig, arXiv:1306.2916
- [19] M. Bochicchio, *et al.*, Nucl. Phys. B **262** (1985) 331
- [20] L. Giusti, *et al.*, Nucl. Phys. B **538** (1999) 249 [hep-lat/9807014]
- [21] F. Karsch, Phys. Rev. D **49** (1994) 3791 [hep-lat/9309022]
- [22] Y. Iwasaki, *et al.*, Phys. Rev. Lett. **78** (1997) 179 [hep-lat/9609022]
- [23] F. Burger, *et al.*, Phys. Rev. D **87** (2013) 074508 [arXiv:1102.4530]
- [24] C. E. Detar and J. B. Kogut, Phys. Rev. Lett. **59** (1987) 399
- [25] M. Cheng, *et al.*, Eur. Phys. J. C **71** (2011) 1564 [arXiv:1010.1216]
- [26] D. Banerjee, R. V. Gavai and S. Gupta, Phys. Rev. D **83** (2011) 074510 [arXiv:1102.4465]
- [27] M. Müller, these proceedings
- [28] A. Bazavov, *et al.* [HotQCD Collaboration], arXiv:1205.3535
- [29] M. I. Buchoff, *et al.*, arXiv:1309.4149